Check for updates

Synergistic effects of fluorine doping on CoPS electrocatalysts for highly efficient hydrogen evolution reaction†

Zhi Dai,[a] Bingrong Wang,[a] Weiwei Li,[a] Yufan Wu, [iD][a] Bingdong Yan*[b] and Kexi Zhang [iD] *[a]

Exploring earth-abundant electrocatalysts for efficient hydrogen evolution reaction (HER) is important for the development of clean and renewable hydrogen energy. Herein, we demonstrated that fluorine anion doping into CoPS significantly enhanced its hydrogen evolution reaction (HER) activity. Controlled fluorination modulated the surface electronic structure of CoPS active sites, forming an optimized F-CoPS electrocatalyst that exhibited superior performance, achieving an overpotential of only 74 mV at 10 mA cm^{-2} and 141 mV at 50 mA cm^{-2}, along with remarkable stability over 50 hours. This study provides a novel and feasible approach to enhance the HER performance of ternary pyrite-type transition-metal phosphosulfides.

Introduction

With the ever-growing demand for energy, it is becoming increasingly important to find new sources of energy that are environmentally friendly. Hydrogen has been well established as one of the most promising renewable energy sources, and efforts are being made to explore advanced approaches to harness its power.[1–4] It is widely believed that electrocatalytic water splitting is an ideal technology for zero-carbon emission hydrogen production. Although precious metals and their oxides are regarded as the best electrocatalysts for HER, their limited abundance and high cost greatly restrict their widespread applications.[5–7] Therefore, investigations into dual-functional catalysts that are abundant in earth resources, efficient, and stable hold great significance for the future of electrochemical water splitting.[8–11]

Transition-metal phosphosulfides (TMPS) have been proven to be excellent HER catalysts in acidic media, as reported in numerous studies.[12–14] However, their intrinsic catalytic activity and electrochemical stability degrade in alkaline medium due to the complexities of the reaction mechanism.[15,16] Currently, heteroatom doping stands as an effective approach to enhance the HER catalytic performance of TMPS.[17–19] While attention has been paid to cation doping, including Co-FePS$_3$,[19] (Cu$_X$Co$_{1-X}$)PS,[20] Ni$_{1-X}$Fe$_X$PS$_3$,[21] anion doping is also promising due to its potential to regulate electron-donating/accepting and metal valence properties.[22] Anions' greater electronegativity enables them to regulate the electronic structure; fluorine, in particular, has the strongest electronegativity, *i.e.*, the most efficient regulation of the electronic structure.[23,24] For instance, Zhou *et al.* discovered that O-doping can effectively assist CoP in catalyzing HER and OER processes. The high relative electronegativity of O can further optimize the electronic structure of CoP, enhance its conductivity, and endow it with superior HER and OER activities.[25] Similarly, Luo *et al.* demonstrated that the strong electronegativity of Se can lead to a decrease in the electron filling degree of the 3d orbitals of the active Co center, thereby enhancing the interaction between water molecules and Co atoms. This, in turn, improves the HER catalytic activity of the catalyst.[26] Later, Ma *et al.* demonstrated that S doping can significantly enhance charge transfer, which, in conjunction with increased active exposure sites, synergistically boosts water electrolysis performance.[27]

In this study, we prepared fluorine-doped CoPS (F-CoPS) nanosheets *via* a three-step synthesis method, combining hydrothermal and high-temperature heat treatments. We investigated the effect of fluorine doping on the surface electronic structure and subsequent HER catalytic performance in alkaline electrolytes. The experimental results indicate that F anion doping significantly improved the HER performance of CoPS, underscoring the practical significance of this strategy in the development of cost-effective and high-performance electrocatalysts.

[a] School of Materials Science and Engineering, Hainan University, Haikou, 570100, China. E-mail: zhangkexi@hainanu.edu.cn

[b] College of Science, Laboratory of Child Cognition & Behavior Development of Hainan Province, Qiongtai Normal University, Haikou, 570100, China

† Electronic supplementary information (ESI) available. See DOI: https://doi.org/10.1039/d4ra08760g

Experimental

Materials preparation

Preparation of Co(CO$_3$)$_{0.5}$OH$_{0.11}$·H$_2$O nanosheets on carbon cloth (CoCH NSs/CC). CoCH NSs/CC was synthesized according

to the method reported by Liu's group.[28] The carbon cloth was cleaned by soaking in nitric solution for 12 h. A solution of $Co(NO_3)_3 \cdot 6H_2O$ and urea in 30 mL deionized water was prepared and sonicated for 30 min. Subsequently, this solution and the cleaned carbon cloth were placed in an autoclave lined with polytetrafluoroethylene. The autoclave was heated in an oven at 120 °C for 8 h. Then, the product was washed three times with deionized water *via* sonication, and dried in an oven at 60 °C for 12 h.

Preparation of CoPS nanosheets on carbon cloth (CoPS NSs/CC). CoPS NSs/CC was synthesized *via* a high temperature heat treatment method. A quartz boat containing 0.015 mol $NaH_2PO_2 \cdot H_2O$ and sulfur powder was placed upstream in a tube furnace, while the as-obtained CoCH NSs/CC was placed downstream and the samples were annealed in a nitrogen atmosphere at 500 °C for 1 h at a ramping rate of 2 °C min^{-1}. After the furnace cooled to room temperature, CoPS NSs/CC was obtained. Control experiments were conducted using varying heat treatment temperatures, marked as CoPS-400, CoPS-500, and CoPS-600. Further, CoPS NSs/CC was calcined with varying ratios of $NaH_2PO_2 \cdot H_2O$ to sulfur powder at 500 °C, which was labeled as CoPS 1 : 3, CoPS 1 : 2, CoPS 1 : 1, CoPS 2 : 1 and CoPS 3 : 1.

Preparation of F-CoPS nanosheets on carbon cloth (F-CoPS NSs/CC). To prepare F-CoPS, the as-obtained CoPS/CC and NH_4F were placed in two different quartz boats. NH_4F was placed upstream, and CoPS/CC was placed downstream. Then, the samples were annealed in a nitrogen atmosphere at 500 °C for 1 h at a ramping rate of 2 °C min^{-1}. F-CoPS NSs/CC was obtained once the furnace naturally cooled to room temperature. For comparison, CoPS NSs/CC was calcined at different temperatures, which was marked as F-CoPS-400, F-CoPS-500, and F-CoPS-600. In addition, CoPS NSs/CC was calcined with different amounts of NH_4F, which was marked as F-CoPS-0.5, F-CoPS-1.0, and F-CoPS-1.5.

Material characterization

The as-prepared materials were characterized by field emission scanning electron microscopy (SEM, Regulus 8100, Japan), transmission electron microscopy (TEM) and high-resolution TEM (HRTEM, Tecnai G2 F20/F30, USA). X-ray diffraction (XRD) measurement was performed on a D8 ADVANCE (Germany). X-ray photoelectron spectroscopy (XPS) data were collected using a Thermo ESCALAB 250XI (USA).

Electrochemical measurements

All electrochemical measurements were performed on an electrochemical workstation (CHI 660E, CH Instruments, Inc.) using a typical three-electrode configuration at room temperature. The electrocatalytic performance was examined in 1 M KOH aqueous solution, using the as-prepared samples as the working electrode, a graphite rod as the counter electrode, and Hg/HgO (in 1 M KOH aqueous solution) as the reference electrode. In addition, the area of all working electrodes was 1 cm^{-2}. For comparison, 20 mg commercial Pt/C was dispersed in 1 mL isopropanol and 5 μL 5% Nafion and ultrasonicated for at least 30 min until a uniform solution was formed. Then, the uniform solution was added to cleaned carbon cloth dropwise. All polarization curves were measured at a scan rate of 5 mV s^{-1} and corrected for the ohmic potential drop (iR). Electrochemical impedance spectroscopy (EIS) measurements were performed at 100 mV overpotential in the range of 100 kHz to 0.01 Hz. The electric double-layer capacitance (C_{dl}) was measured at different scan rates in the range of 20 to 100 mV s^{-1}. The chronopotentiometric durability test was performed at a current density of 10 mA cm^{-2} for 25 h. Electrochemical voltage (E *vs.* Hg/HgO reference electrode) was converted to the reversible hydrogen electrode (RHE) scale at pH 14 using the Nernst equation, $E(RHE) = E(Hg/HgO) + E^{\ominus}(Hg/HgO) + 0.059$ pH.

Results and discussion

The F-CoPS nanosheet catalyst was prepared through a three-step procedure, as presented in Fig. 1. The obtained precursor and catalysts were analyzed by XRD, with the results shown in Fig. 2. The typical XRD pattern recorded CoCH (Fig. 2a) shows the main diffraction peaks located at 2θ values of 24.13°, 28.69°, 30.36°, 33.77°, 35.25°, and 39.48°, which can be assigned to the
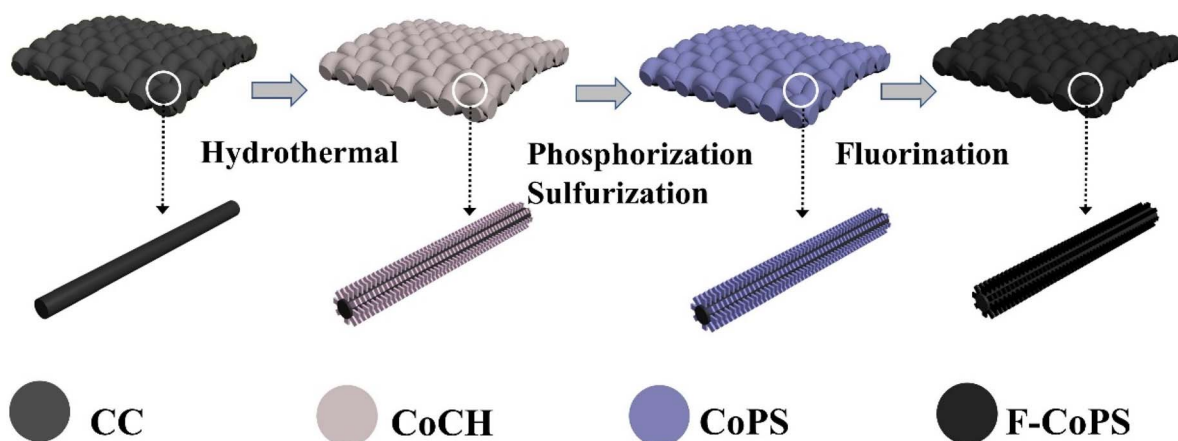

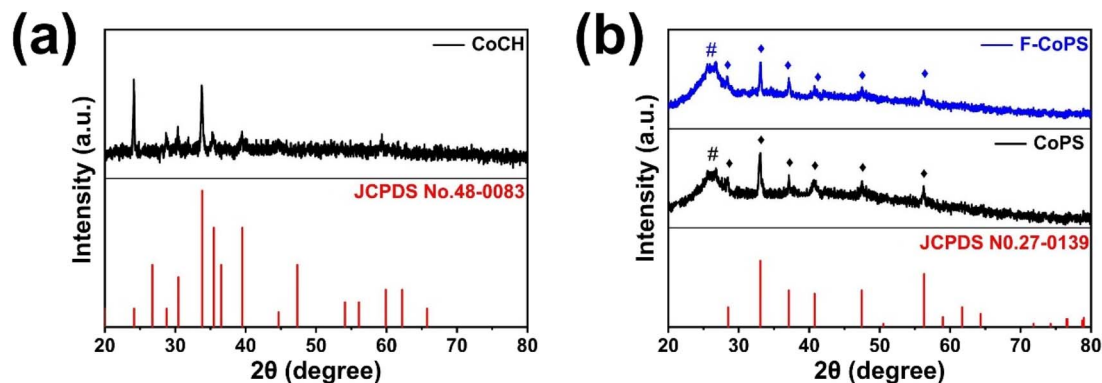Fig. 1 Schematic of the preparation of the F–CoPS nanosheet catalyst.

Fig. 2 X-ray diffraction patterns of (a) CoCH nanosheets, (b) CoPS nanosheets and F–CoPS nanosheets.

(111), (121), (300), (221), (040) and (231) planes of CoCH (JCPDS No. 48-0083), respectively, confirming the successful preparation of the precursor.

The X-ray diffraction (XRD) pattern in Fig. 2b exhibits the main diffraction peaks of CoPS located at 28.51°, 33.03°, 37.13°. 40.76°. 47.45°, and 56.28°, which can be assigned to the (111),

(200), (210), (211), (220) and (311) planes of CoPS (JCPDS No. 27-0139), respectively, demonstrating the successful transformation from CoCH to CoPS following the heat treatment synthesis process.[29] To determine the optimal synthesis conditions, we calcined the CoCH precursor at different temperatures (400 °C, 500 °C, and 600 °C) at a $NaH_2PO_2 \cdot H_2O$: sulfur powder
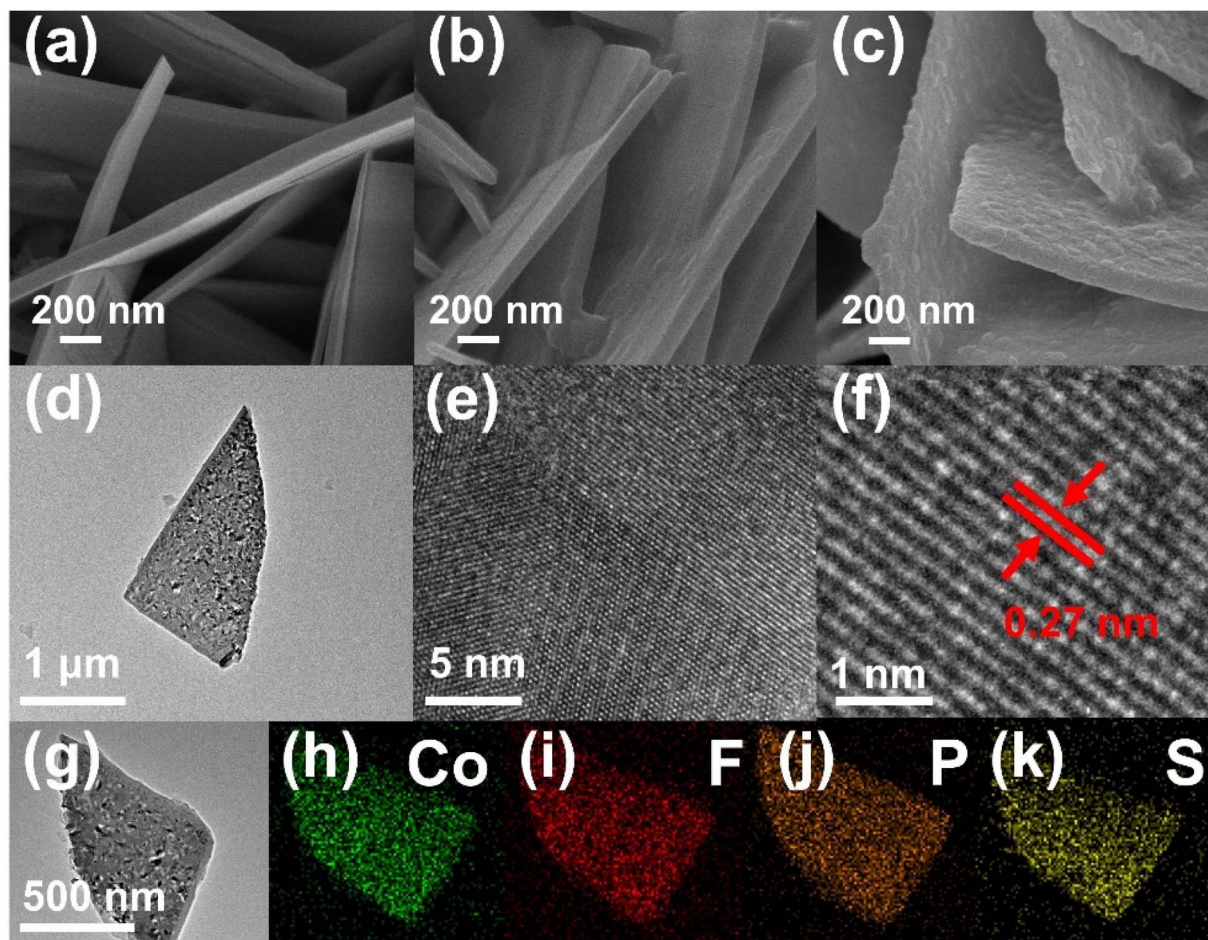

Fig. 3 Morphology and chemical composition. Typical SEM images of (a) CoCH, (b) CoPS, and (c) F–CoPS. (d) TEM image, (e) and (f) high-resolution TEM images. (g) Dark-field TEM image and corresponding elemental mapping images of (h) Co, (i) F, (j) P, and (k) S elements for F–CoPS nanosheet.

ratio of 1:1. The XRD patterns of CoPS-400, CoPS-500 and CoPS-600 in Fig. S1† are also consistent with the standard diffraction cards of CoPS (PDF#27-0139). Subsequently, we explored five different ratios of $NaH_2PO_2 \cdot H_2O$ and sulfur powders (1:3, 1:2, 1:1, 2:1, and 3:1) to determine the best ratio. As shown in Fig. S2,† the diffraction peaks of CoPS with different ratios retained the crystal structure of CoPS (PDF#27-0139). In addition, the influence of different fluorination temperatures and the amount of NH_4F was examined, as shown in Fig. S3 and S4,† respectively. It was found that fluorination did not affect the crystal structure of the materials, demonstrating the successful F anion doping and the stability of the synthesized material. Furthermore, the morphology of the materials was investigated using SEM (Fig. 3a–c).

Fig. 3a indicates the self-supporting growth of CoCH nanosheets on the carbon cloth with a smooth and highly uniform surface. Upon completion of the second step, their structure and morphology exhibited a minor change with roughened surface (Fig. 3b), indicating the formation of CoPS nanosheets. Further fluorination led to an even rougher surface (Fig. 3c). The TEM and HRTEM analysis (Fig. 3d–f) further revealed the uniform microstructure of the F-CoPS nanosheet, with distinct lattice stripes of approximately 0.27 nm, corresponding to the (200) planes of CoPS, which is consistent with the XRD results. Hence, it is clear that the nanosheets are composed of F-CoPS. Energy dispersive X-ray (EDX) elemental mapping was utilized to confirm the chemical composition and elemental distribution of F-CoPS (Fig. 3g), demonstrating a homogeneous distribution of Co, F, P and S throughout the nanosheets. The EDX

spectrum of F-CoPS is presented in Fig. S5,† confirming that this composite is composed of Co, P, S and F elements.

The electronic state and the chemical environment of the surface elements were examined using XPS analysis, confirming that Co, F, P and S are the only four elements present in the sample. As illustrated in Fig. 4a, the Co 2p spectra of CoPS show two peaks located at 781.4 and 797.4 eV, which are ascribed to Co^{3+}, and peaks at 783.6 and 799.9 eV, corresponding to Co^{2+}. In the Co 2p spectra of F-CoPS, two peaks were observed at 781.9 eV and 798.2 eV, corresponding to Co^{3+}, and two other peaks at 784.3 eV and 800.6 eV, which are assigned to Co^{2+}.[30] In addition, the satellite peaks centered at 787.5 and 803.6 eV are due to the shaking excitation of high-spin Co^{2+}.[31–34] It is evident that F doping induced a positive shift in the Co 2p binding energy, indicating the modulation of the electronic structure of the metal. As shown in Fig. 4b, the F 1s spectrum exhibited a characteristic peak at around 687.2 eV, which is indexed to the F–P bond, demonstrating the successful synthesis of the F-CoPS nanosheets. The P 2p high-resolution spectrum of F-CoPS in Fig. 4c shows two characteristic peaks at around 129.8 eV and 130.8 eV, corresponding to P $2p_{3/2}$ and P $2p_{1/2}$ of the P–M bond, respectively.[35] It is noteworthy that the positive shift of approximately 0.3 eV in the P 2p binding energy in F-CoPS relative to CoPS (Fig. 4c) is consistent with the higher electronegativity of F than that of P.[36] The presence of a P–O peak at 134.4 eV for both samples is attributed to the surface oxidation,[37,38] and the characteristic peak at 135.3 eV is attributed to the F–P bond after fluorination.[23] In the S 2p XPS spectra (Fig. 4d), CoPS and F-CoPS are very similar, showing peaks
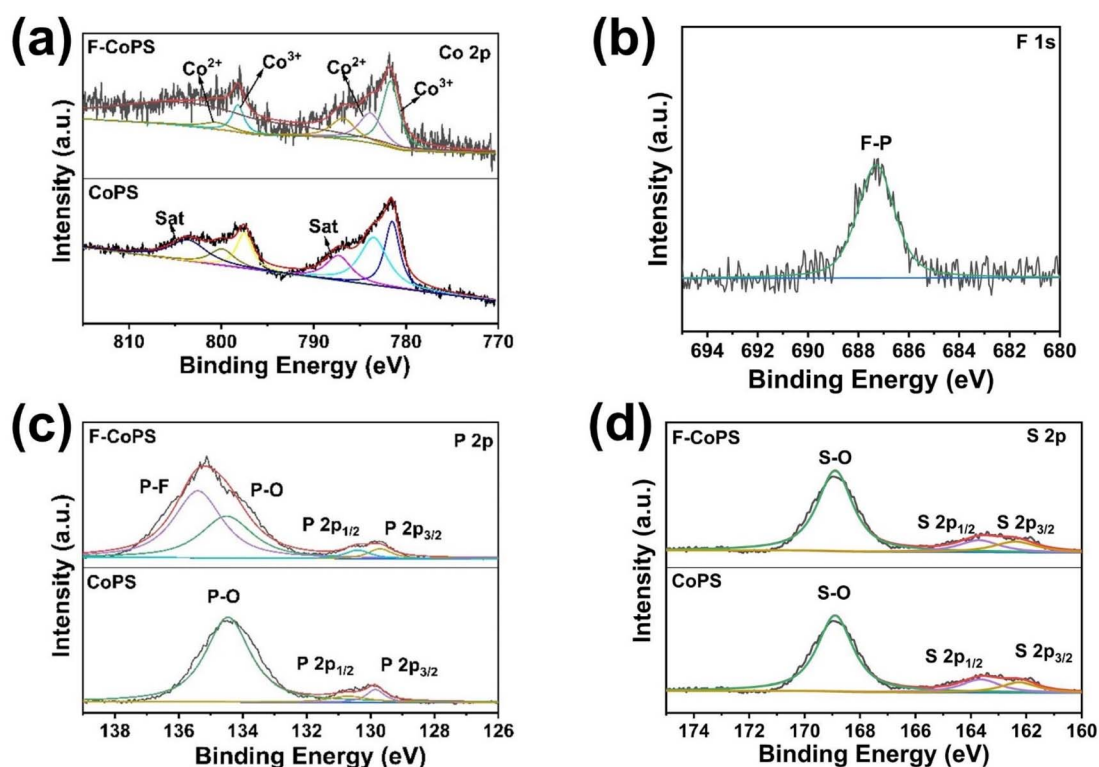

Fig. 4 X-ray photoelectron spectral regions for (a) Co 2p, (b) F 1s, (c) P 2p and (d) S 2p levels of CoPS and F-CoPS.

centered at 162.2 eV and 163.7 eV, which are indexed to S $2p_{3/2}$ and S $2p_{1/2}$, respectively, and a surface S–O peak at 169.0 eV.[39] These observations in the P 2p binding energy, together with the unchanged S 2p features, indicate the successful F-doping and modification of the electron structure, thus facilitating the catalytic performance of the electrocatalyst. In addition, Fig. S6† indicates that the oxygen in the material originates from the adsorbed air oxygen, not from the material itself, and the material did not undergo oxidation.

The catalytic activities of CoP@NC for HER were tested in an alkaline electrolyte with a three-electrode system and the catalytic activities of CoPS and Pt/C (coated on cleaned carbon cloth) were also investigated for comparison. As illustrated in Fig. S7 and S8,† 500 °C is the optimal reaction temperature at which CoPS-500 exhibited the best HER catalytic activity with the lowest overpotential, lowest Tafel slope, lowest charge transfer resistance and largest double-layer capacitance (C_{dl}). Fig. S9 and S10† show that CoPS at 1 : 1 is the optimal ratio, which showcased the lowest overpotential, lowest Tafel slope, lowest charge transfer resistance and largest C_{dl}. Further, different fluorination temperatures as well as the amount of NH_4F were investigated, with 500 °C determined to be the optimal fluorination temperature, as shown in Fig. S11 and S12,† and 1.0 g as the optimal amount of NH_4F, as shown in Fig. S13 and S14.† As expected, F-CoPS exhibited excellent catalytic activity with η_{10} of 74 mV and η_{50} of 141 mV, which are significantly lower than that of CoPS (η_{10} = 142 mV and η_{50} = 207 mV) and higher than that of Pt/C (η_{10} = 15 mV and η_{50} = 55 mV), as presented in Fig. 5a.
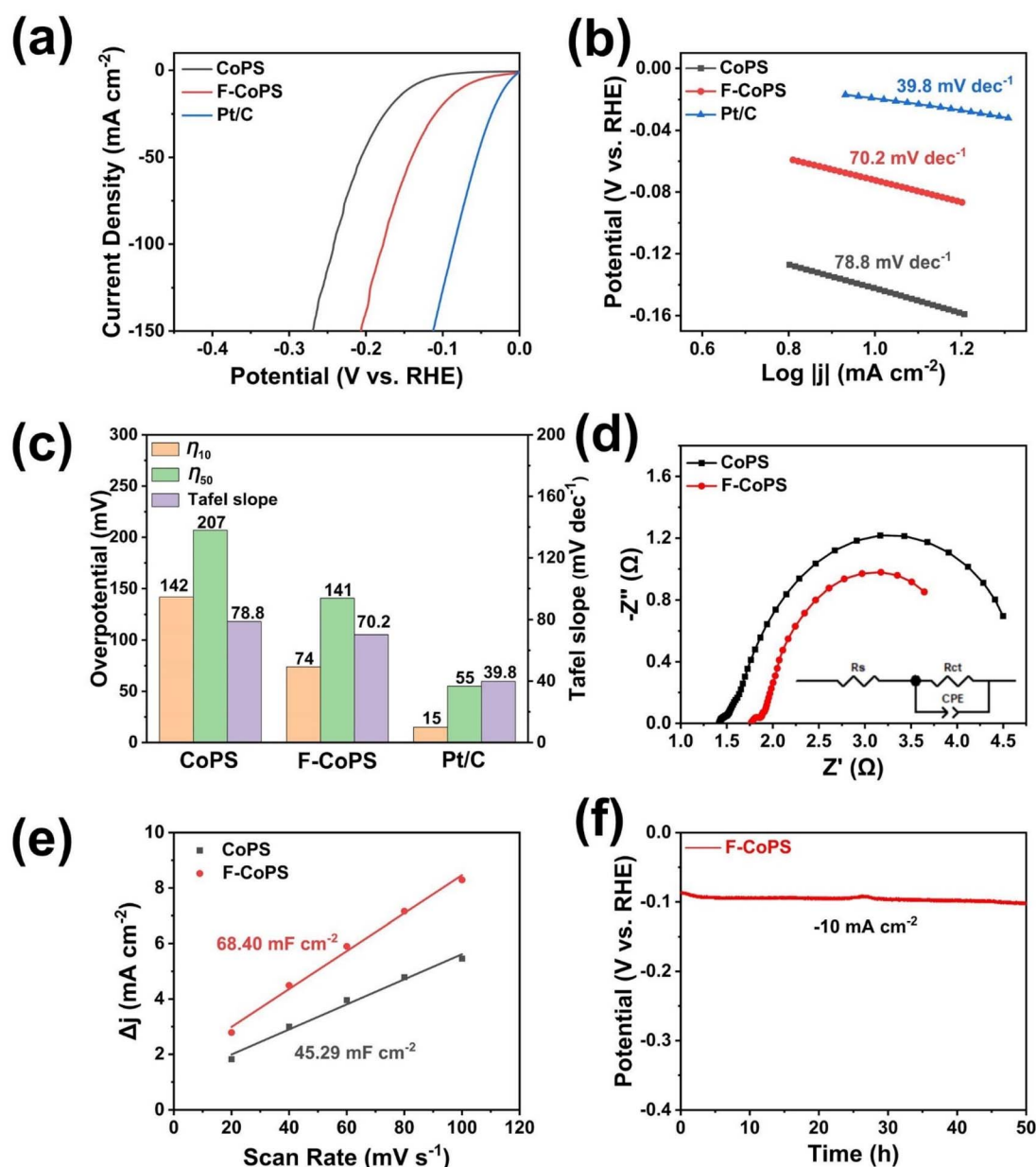

Fig. 5 (a) LSV curves, (b) Tafel slopes, (c) summary of the overpotentials and Tafel slopes of CoPS, F-CoPS and Pt/C catalysts, (d) EIS spectra of CoPS and F-CoPS, (e) C_{dl} values of CoPS and F-CoPS, and (f) chronopotentiometric curves of F-CoPS for the HER in 1 M KOH solution.
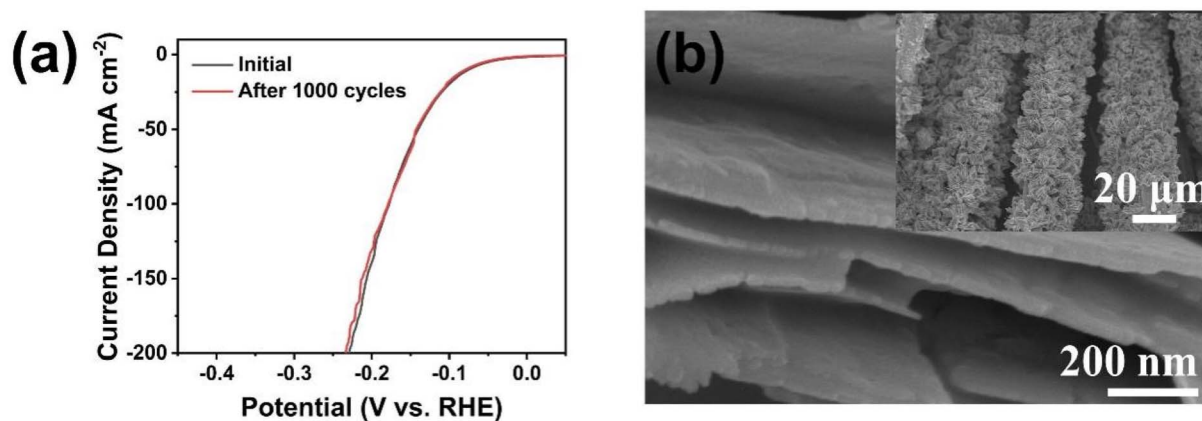
Fig. 6 (a) Initial and after 1000 cycles polarization curves of F–CoPS in 1.0 M KOH. (b) SEM images of F–CoPS after long-time testing.

Additionally, the reaction kinetics of HER were evaluated using Tafel analysis (Fig. 5b), electrochemical impedance spectroscopy (EIS, Fig. 5d), and electrochemical active surface area (ECSA) measurements (Fig. S15†). In addition, the specific activity (ECSA normalized current density) was calculated, as shown in Fig. S16,† demonstrating that the intrinsic activity of the F-CoPS catalyst exceeded that of CoPS under the same conditions. To ensure the reproducibility, we used a saturated calomel electrode and Ag|AgCl (saturated KCl solution) electrode as the reference electrodes to test the HER performance of the catalyst. As shown in Fig. S17,† the polarization curves obtained by using different reference electrodes are almost the same. In addition, all the R_{ct} and R_s values of catalysts are shown in Table S1.† Compared with the other electrodes, F-CoPS possesses the smallest R_{ct} (2.432 Ω) and smallest R_s (1.499 Ω), which indicates that F ion doping can significantly promote the HER kinetics and charge transfer process. The Tafel slopes of CoPS and F-CoPS are 78.8 mV dec^{-1} and 70.2 mV dec^{-1}, respectively, which are higher than that of Pt/C (39.8 mV dec^{-1}). All the electrochemical data of the as-obtained catalysts are presented in Fig. 5c. EIS was performed to investigate the kinetics of the mass transfer and charge transfer on the electrocatalysts[40] (Fig. 5d). F-CoPS exhibited lower transfer resistance (R_{ct}) compared to CoPS. The ECSA is another important indicator for assessing the electrocatalytic activity of materials.[41,42] Thus, the ECSA was evaluated via a simple cyclic voltammetry (CV) method in the range of 0.1–0.2 V (vs. RHE) at different scan rates (20–100 mV s^{-1}) (Fig. S15†), where C_{dl} of F-CoPS was 68.40 mF cm^{-2}, higher than CoPS, indicating a larger ECSA and a greater number of active sites available on F-CoPS. Fig. 5f demonstrates the excellent stability of F-CoPS with negligible degradation for 50 h. The durability of F-CoPS was further investigated via cyclic voltammetry (CV) in 1 M KOH (0 to −0.13 V vs. RHE, 50 mV s^{-1}, 1000 cycles). The cathodic current density of the polarization curve shows no significant decrease compared to the initial curve (Fig. 6a). In addition, the SEM images (Fig. 6b) of F-CoPS demonstrate its morphological stability, which retained its structure after 1000 cycles, suggesting its excellent electrochemical durability. As shown in Fig. S18,† the intensity of the diffraction peaks of F-CoPS was

weakened, but its crystal phase structure could still be observed, which proves the stability of the catalyst. The XPS spectra of F-CoPS after the HER stability test were also recorded. Fig. S19(a)† presents the XPS spectrum after the HER stability test, where the peaks of Co 2p shifted to a lower binding energy due to the cathodic reduction reaction.[43] As shown in Fig. S19(b),† the weakening of the F peak may be due to the surface dissolution phenomenon of the F–P bond during the reaction. As displayed in Fig. S19(c) and (d),† in the P 2p and S 2p spectra after HER, phosphides can still be observed. Thus, all the results after the HER stability test show that the material has excellent electrochemical durability.

Conclusions

We successfully synthesized an anionic F-doped catalyst (F-CoPS) through a three-step procedure, which exhibited an excellent intrinsic HER electrocatalytic performance, with its optimal catalytic performance achieved at a 1 : 1 molar ratio of $NaH_2PO_2 \cdot H_2O$: sulfur powder at 500 °C, together with 1.0 g of NH_4F at 500 °C. The outstanding intrinsic HER performance of the F-CoPS nanosheets was validated by their low overpotential of 74 mV at 10 mA cm^{-2} in alkaline medium. This enhancement compared to the individual CoPS nanosheet catalyst stems from the F-doping-induced modulation of the Co electronic structure. Also, the long-term electrochemical stability of the F-CoPS nanosheets for up to 50 h confirmed that they are a promising HER electrocatalyst. Thus, this work demonstrated that F anion doping is a promising strategy to improve the HER catalytic activity of TMPS in alkaline media.

Data availability

The data supporting this article have been included as part of the ESI.†

Conflicts of interest

There are no conflicts to declare.

Acknowledgements

References

1 W. Seh Zhi, J. Kibsgaard, F. Dickens Colin, I. Chorkendorff, K. Nørskov Jens and F. Jaramillo Thomas, *Science*, 2017, **355**, eaad4998.

2 S. Q. Lu and Z. B. Zhuang, *Sci. China Mater.*, 2016, **59**, 217–238.

3 J. A. Turner, *Science*, 2004, **305**, 972–974.

4 Y. J. Bao, H. F. Ru, Y. F. Wang, K. X. Zhang, R. T. Yu, Q. Wu, A. M. Yu, D. S. Li, C. H. Sun, W. W. Li and J. C. Tu, *Adv. Funct. Mater.*, 2024, **34**, 11.

5 J. X. Fan, H. X. Du, Y. Zhao, Q. Wang, Y. N. Liu, D. Q. Li and J. T. Feng, *ACS Catal.*, 2020, **10**, 13560–13583.

6 J. H. Kim, D. Shin, J. Lee, D. S. Baek, T. J. Shin, Y. T. Kim, H. Y. Jeong, J. H. Kwak, H. Kim and S. H. Joo, *ACS Nano*, 2020, **14**, 1990–2001.

7 B. Y. Zhang, W. W. Li, K. X. Zhang, J. T. Gao, Y. Cao, Y. Q. Cheng, D. L. Chen, Q. Wu, L. Ding, J. C. Tu, X. L. Zhang and C. H. Sun, *J. Mater. Sci. Technol.*, 2024, **177**, 214–223.

8 Y. J. Li, Y. J. Sun, Y. N. Qin, W. Y. Zhang, L. Wang, M. C. Luo, H. Yang and S. J. Guo, *Adv. Energy Mater.*, 2020, **10**, 20.

9 Q. Zhao, Z. H. Yan, C. C. Chen and J. Chen, *Chem. Rev.*, 2017, **117**, 10121–10211.

10 L. Z. Bu, N. Zhang, S. J. Guo, X. Zhang, J. Li, J. L. Yao, T. Wu, G. Lu, J. Y. Ma, D. Su and X. Q. Huang, *Science*, 2016, **354**, 1410–1414.

11 M. L. Guo, Z. Y. Wu, M. M. Zhang, Z. J. Huang, K. X. Zhang, B. R. Wang and J. C. Tu, *Rare Met.*, 2023, **42**, 1847–1857.

12 M. Caban-Acevedo, M. L. Stone, J. R. Schmidt, J. G. Thomas, Q. Ding, H. C. Chang, M. L. Tsai, J. H. He and S. Jin, *Nat. Mater.*, 2015, **14**, 1245–1251.

13 N. Mahmood, Y. D. Yao, J. W. Zhang, L. Pan, X. W. Zhang and J. J. Zou, *Adv. Sci.*, 2018, **5**, 23.

14 M. Wang, A. Saad, X. G. Li, T. Peng, Q. T. Zhang, M. Kumar and W. Zhao, *Dalton Trans.*, 2021, **50**, 12870–12878.

15 Y. Zheng, Y. Jiao, A. Vasileff and S. Z. Qiao, *Angew. Chem., Int. Ed.*, 2018, **57**, 7568–7579.

16 Y. Chen, Y. Rao, R. Z. Wang, Y. A. Yu, Q. L. Li, S. J. Bao, M. W. Xu, Q. Yue, Y. N. Zhang and Y. J. Kang, *Nano Res.*, 2020, **13**, 2407–2412.

17 D. Rakov, Y. Z. Li, S. Q. Niu and P. Xu, *J. Alloys Compd.*, 2018, **769**, 532–538.

18 Z. P. Yu, Y. F. Li, V. Martin-Diaconescu, L. Simonelli, J. R. Esquius, I. Amorim, A. Araujo, L. J. Meng, J. L. Faria and L. F. Liu, *Adv. Funct. Mater.*, 2022, **32**, 12.

19 S. Wang, B. B. Xiao, S. J. Shen, K. Song, Z. P. Lin, Z. P. Wang, Y. C. Chen and W. W. Zhong, *Nanoscale*, 2020, **12**, 14459–14464.

20 P. P. Patel, O. I. Velikokhatnyi, S. D. Ghadge, P. J. Hanumantha, M. K. Datta, R. Kuruba, B. Gattu, P. M. Shanthi and P. N. Kumta, *Int. J. Hydrogen Energy*, 2018, **43**, 7855–7871.

21 B. Song, K. Li, Y. Yin, T. Wu, L. N. Dang, M. Cabán-Acevedo, J. C. Han, T. L. Gao, X. J. Wang, Z. H. Zhang, J. R. Schmidt, P. Xu and S. Jin, *ACS Catal.*, 2017, **7**, 8549–8557.

22 Y. D. Liu, P. Vijayakumar, Q. Y. Liu, T. Sakthivel, F. Y. Chen and Z. F. Dai, *Nano-Micro Lett.*, 2022, **14**, 41.

23 D. X. Xu, J. Yao, X. Z. Ma, Y. Xiao, C. Zhang, W. Lin and H. Gao, *J. Colloid Interface Sci.*, 2022, **619**, 298–306.

24 J. W. Zhu, J. Q. Chi, T. Cui, L. L. Guo, S. Q. Wu, B. Li, J. P. Lai and L. Wang, *Appl. Catal., B*, 2023, **328**, 10.

25 G. Y. Zhou, M. Li, Y. L. Li, H. Dong, D. M. Sun, X. Liu, L. Xu, Z. Q. Tian and Y. W. Tang, *Adv. Funct. Mater.*, 2020, **30**, 8.

26 Y. N. Men, Y. Tan, P. Li, X. M. Cao, S. F. Jia, J. B. Wang, S. L. Chen and W. Luo, *Appl. Catal., B*, 2021, **284**, 7.

27 L. Z. Ma and J. X. Guo, *Mater. Lett.*, 2022, **307**, 4.

28 S. D. Liu, Y. Yin, Y. Shen, K. S. Hui, Y. T. Chun, J. M. Kim, K. N. Hui, L. P. Zhang and S. C. Jun, *Small*, 2020, **16**, 14.

29 Z. G. Niu, C. Qiu, J. Jiang and L. H. Ai, *ACS Sustainable Chem. Eng.*, 2019, **7**, 2335.

30 S. L. Yang, L. Peng, E. Oveisi, S. Bulut, D. T. Sun, M. Asgari, O. Trukhina and W. L. Queen, *Chem.–Eur. J.*, 2018, **24**, 4234–4238.

31 Y. R. Hao, H. Xue, J. Sun, N. K. Guo, T. S. Song, J. W. Sun and Q. Wang, *ACS Appl. Mater. Interfaces*, 2021, **13**, 56035–56044.

32 D. He, X. Y. Song, W. Q. Li, C. Y. Tang, J. C. Liu, Z. J. Ke, C. Z. Jiang and X. H. Xiao, *Angew. Chem., Int. Ed.*, 2020, **59**, 6929–6935.

33 J. Z. Liu, Y. F. Ji, J. W. Nai, X. G. Niu, Y. Luo, L. Guo and S. H. Yang, *Energy Environ. Sci.*, 2018, **11**, 1736–1741.

34 H. Chen, J. Chen, P. Ning, X. Chen, J. Liang, X. Yao, D. Chen, L. Qin, Y. Huang and Z. Wen, *ACS Nano*, 2021, **15**, 12418–12428.

35 Y. Pan, Y. Q. Liu, Y. Lin and C. G. Liu, *ACS Appl. Mater. Interfaces*, 2016, **8**, 13890–13901.

36 Y. K. Sun, W. Y. Sun, L. H. Chen, A. L. Meng, G. C. Li, L. Wang, J. F. Huang, A. L. Song, Z. H. Zhang and Z. J. Li, *Nano Res.*, 2023, **16**, 228–238.

37 X. W. Yu, J. Zhao and M. Johnsson, *Adv. Funct. Mater.*, 2021, **31**, 2101578.

38 W. Z. Chen, P. Y. Liu, L. Zhang, Y. Liu, Z. L. Liu, J. L. He and Y. Q. Wang, *Chem. Eng. J.*, 2021, **424**, 12.

39 K. L. Zhang, T. W. Zhang, J. W. Liang, Y. C. Zhu, N. Lin and Y. T. Qian, *RSC Adv.*, 2015, **5**, 14828–14831.

40 D. Merki, H. Vrubel, L. Rovelli, S. Fierro and X. L. Hu, *Chem. Sci.*, 2012, **3**, 2515–2525.

41 Y. Pan, K. A. Sun, S. J. Liu, X. Cao, K. L. Wu, W. C. Cheong, Z. Chen, Y. Wang, Y. Li, Y. Q. Liu, D. S. Wang, Q. Peng, C. Chen and Y. D. Li, *J. Am. Chem. Soc.*, 2018, **140**, 2610–2618.

42 D. Bohm, M. Beetz, C. Kutz, S. Y. Zhang, C. Scheu, T. Bein and D. Fattakhova-Rohlfing, *Chem. Mater.*, 2020, **32**, 10394–10406.

43 X. T. Yuan, H. X. Ge, X. Wang, C. L. Dong, W. J. Dong, M. S. Riaz, Z. W. Xu, J. X. Zhang and F. Q. Huang, *ACS Energy Lett.*, 2017, **2**, 1208–1213.